Attosecond electron interferometry for measurement of the quantum phase of free-electron wave packets

Candong Liu[*] and Mauro Nisoli

Department of Physics, Politecnico di Milano, National Research Council of Italy, Institute of Photonics and Nanotechnologies (CNR-IFN), Piazza L. da Vinci 32, 20133 Milano, Italy
(Received 18 September 2012; published 5 November 2012)

Single-photon ionization of a hydrogen atom irradiated by two time-delayed isolated attosecond pulses is theoretically investigated by numerically solving the fully three-dimensional time-dependent Schrödinger equation. It is demonstrated that the analysis of the angular-resolved electron energy spectrum, showing a complex interference pattern, allows one to completely retrieve the difference between the energy-dependent phases of the electron wave packets generated by the two delayed attosecond pulses. Moreover, it is shown that in the case of a pair of excitation pulses with the same chirp rate, the proposed interferometric technique can be used to measure the difference between the carrier envelope phase values of two attosecond pulses.

I. INTRODUCTION

Since the first experimental demonstration of the generation of attosecond pulses [1,2], various experimental techniques have been proposed and implemented for the measurement of the subfemtosecond electron dynamics in atoms, molecules, and solids [3,4]. Trains of attosecond pulses have been used, in combination with infrared pulses in pump-probe configurations, to observe the interference of transiently bound electron wave packets (EWPs) in strongly driven atomic systems [5,6]. Attosecond electron wave packet interferometry, based on the use of a train of attosecond pulses and an infrared field, which induces a momentum shear between the consecutive EWPs generated by each attosecond pulse, has been implemented for the measurement of the phase variation of EWPs in momentum space [7]. More recently, isolated attosecond pulses have been used for the characterization of attosecond EWPs using an interferometric pump-probe scheme [8]. In this case, a free EWP, generated in the continuum, was used as a reference to characterize a bound EWP generated by the excitation of helium atoms with isolated attosecond pulses. In a different case, when the photon energy of the attosecond pulses is above the ionization potential of the target atoms, the spectral phase of the extreme ultraviolet (XUV) pulses is directly mapped onto the free EWP [9], so that the chirp of the attosecond pulse leads to a phase contribution to the EWP, with important consequences for the analysis of the experimental results obtained by using the attosecond interferometric techniques. Note that attosecond pulses present an intrinsic chirp, due to the harmonic photon emission associated with different electron excursion times [10,11], which can be compensated for or adjusted by using various techniques.

In this work, we investigate the photoionization of a hydrogen atom driven by two isolated attosecond pulses with variable temporal delay. The photoionization leads to the generation of two interfering EWPs. The interference pattern is calculated as a function of the delay between the two attosecond pulses by numerically solving the fully three-dimensional time-dependent Schrödinger equation ((3)

D-TDSE), assuming that the pulses are characterized by arbitrary chirp rates and a carrier envelope phase (CEP). Essential features of the interferogram are obtained by a simple analytical approach. A method is proposed to completely retrieve the difference between the energy-dependent phases of the EWP generated by the two XUV pulses. It is also shown that, in the case of attosecond pulses with the same chirp, the proposed technique can be used for the measurement of the difference between the CEP values of two attosecond pulses.

II. THEORETICAL MODEL AND NUMERICAL METHODS

The interaction of XUV attosecond pulses and a hydrogen atom can be investigated by using the fully 3D-TDSE in the Cartesian spherical coordinates, given by

$$i\frac{\partial}{\partial t}\psi(\mathbf{r},t) = \left[-\frac{1}{2}\frac{1}{r^2}\frac{\partial}{\partial r}r^2\frac{\partial}{\partial r} + \frac{\hat{\ell}^2}{2r^2} - \frac{1}{r} + V_I(\mathbf{r},t)\right]\psi(\mathbf{r},t),$$

(1)

where $\hat{\ell}^2$ is the square of the orbit angular momentum operator and $V_I(\mathbf{r},t)$ describes the interaction of the atom with the applied XUV pulse. Atomic units will be used in the work: $e = \hbar = m_e = 1$, where e and m_e are the electron charge and mass, respectively. The vector potential of a chirped Gaussian attosecond pulse, j, with linear polarization along the z axis can be written as [12]

$$\mathbf{A}_j(t) = \text{Re}\left\{-i\frac{\sqrt{I_j}}{\omega_j}\exp\left[-i[\omega_j(t-t_j) + \varphi_j]\right.\right.$$
$$\left.\left. - 2\ln 2\frac{(t-t_j)^2}{\tau_j^2(1-i\xi_j)}\right]\right\}\mathbf{e}_z,$$

(2)

where I_j is the peak intensity, t_j is the temporal coordinate, which corresponds to the peak of the pulse envelope, ω_j is the central carrier frequency at $t = t_j$, ξ_j is the dimensionless linear chirp rate, τ_j is the pulse duration (full width at half-maximum) for the transform-limited pulse ($\xi_j = 0$), and φ_j is the CEP. The pulse duration of the chirped pulse is given by $\tau_{j,\text{chirp}} = \tau_j\sqrt{1 + \xi_j^2}$, without any modification of the pulse spectral profile. The total time-dependent vector

potential of two chirped and temporally delayed XUV pulses can be written as $\mathbf{A}(t) = \mathbf{A}_1(t) + \mathbf{A}_2(t)$. In the length gauge and in the dipole approximation, the interaction Hamilton in Eq. (1) can therefore be expressed as $V_I(\mathbf{r},t) = -\mathbf{r} \cdot d\mathbf{A}(t)/dt$. A detailed description of the numerical method used to solve Eq. (1) is reported in Ref. [13]. Upon using the expansion of the time-dependent wave function $\psi(\mathbf{r},t)$ in a series of partial waves, Eq. (1) can be reduced to a set of coupled equations between the different angular quantum numbers for the radial wave function [14]. The five-point central finite-difference scheme is employed to discretize the radial equations [15]. The temporal evolution of the wave function is carried out by the Arnoldi-Lanczos algorithm. In our calculation, the simulation parameters are the same as those in Ref. [13], which ensures that all the results fully converge.

The probability amplitude, $a(\mathbf{p})$, of the continuum electron wave packet with momentum $\mathbf{p} = (p,\theta_p,\phi_p)$ generated by the XUV pulse is calculated by projecting the final wave function onto the field-free Coulomb continuum state. For the hydrogen atom with the Coulomb potential, an analytical formula can be obtained to calculate $a(p,\theta_p,\phi_p)$ [13]. Because of the axial symmetry of the wave function, $a(p,\theta_p,\phi_p)$ is independent of the azimuth angle ϕ_p so that the angular-resolved electron energy spectrum can be described by the double differential ionization probability (DDIP):

$$D(\mathcal{E},\theta_p) = \frac{\partial^2 P}{\partial\mathcal{E}\sin\theta_p\partial\theta_p} = 2\pi\sqrt{2\mathcal{E}}\,|a(\sqrt{2\mathcal{E}},\theta_p,0)|^2, \quad (3)$$

where $\mathcal{E} = p^2/2$ is the kinetic energy of the photoelectron.

III. RESULTS AND DISCUSSION

A. Interference spectrogram from TDSE calculation

We have first calculated $D(\mathcal{E},\theta_p)$ upon scanning the temporal delay between the two attosecond pulses. The total electric field of the XUV pulses is shown in Fig. 1, where both pulses have the same peak intensity $I_1 = I_2 = 1 \times 10^{12}$ W/cm^2, central carrier frequency $\omega_1 = \omega_2 = 36$ eV, transform-limited

FIG. 1. (Color online) Electric field of two delayed isolated attosecond pulses used to photoionize a hydrogen atom. The XUV pulses have the same peak intensity $I_1 = I_2 = 1 \times 10^{12}$ W/cm^2, central carrier frequency $\omega_1 = \omega_2 = 36$ eV, transform-limited duration $\tau_1 = \tau_2 = 130$ as, and different chirp rates $\xi_1 = -2, \xi_2 = 3$ and CEP values $\varphi_1 = 0$, $\varphi_2 = \pi/2$. The electric field evolution is reported in atomic units (a.u.).
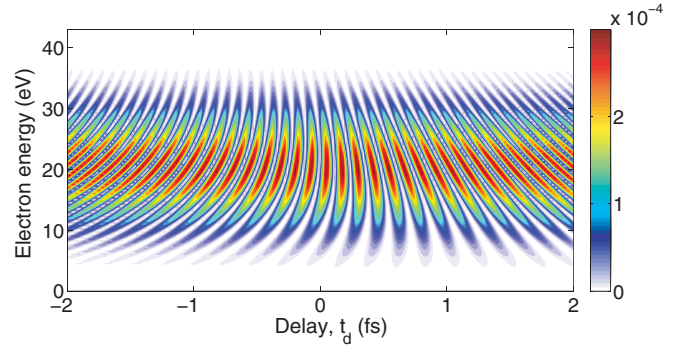
FIG. 2. (Color online) Double differential ionization probability (DDIP) map (electron spectrogram) for electrons emitted along the $\theta_p = 0$ direction as a function of electron energy and temporal delay between the two attosecond pulses. The parameters of the XUV pulses are the same as in Fig. 1.

duration $\tau_1 = \tau_2 = 130$ as, and different chirp rates $\xi_1 = -2$, $\xi_2 = 3$, and CEP values $\varphi_1 = 0, \varphi_2 = \pi/2$. These pulse parameters can be achieved experimentally by using, for example, the polarization gating technique [16]. The temporal delay between the two pulses is defined as $t_d = t_2 - t_1$, so that in the case of positive (negative) delay, pulse 1 (2) precedes pulse 2 (1). Figure 2 shows the DDIP $D(\mathcal{E},\theta_p)$ as a function of the electron energy, $\mathcal{E}$, and of the delay t_d. Here, $\theta_p = 0$ is used in the calculation in order to consider only those electrons emitted along the laser polarization direction. The spectrogram shows a series of tilted interference fringes, whose spacing in energy decreases as the delay increases. It is possible to demonstrate that important information can be extracted by Fourier analysis of the delay-dependent spectrogram. Figure 3(a) shows the spectrogram in the energy-energy representation, obtained by calculating the Fourier transform of the DDIP at each electron energy, thus obtaining a two-dimensional function of the electron energy and the Fourier frequency, ω'. In this representation, the spectrogram exhibits a linear increase with ω'. The spectrogram can be also analyzed by using a time-time representation, as shown in Fig. 3(b). In this case, the Fourier transform is calculated along the energy axis for each temporal delay. By using this representation, the spectrogram shows an X shape and a horizontal linear region with oscillations around the zero delay.

B. Analytical investigation

To understand the main features of the spectrogram in the different representations, it is possible to use a simple analytical model to describe the ionization process induced by the two attosecond pulses. Assuming that both pulses create free EWPs, the probability amplitude for the total EWP in the spectral domain can be expressed as

$$M(\omega) = M_1(\omega)e^{i\phi_1(\omega)} + M_2(\omega)e^{i\phi_2(\omega)}, \quad (4)$$

where $M_j(\omega)$ and $\phi_j(\omega)$ $(j = 1,2)$ are the frequency-dependent amplitude and phase of the EWP created by the XUV pulse j. The generated spectrogram, $I(\omega,t_d)$, which is a two-dimensional function of electron energy, ω, and delay, t_d,
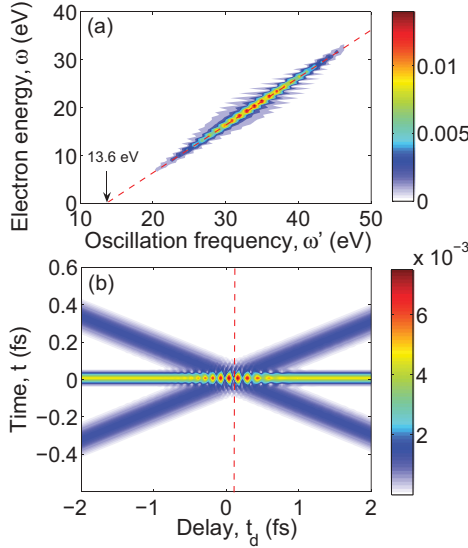
FIG. 3. (Color online) (a) Energy-energy representation of the electron spectrogram obtained from Fourier analysis of the map shown in Fig. 2. The red dashed line was obtained by the analytical approach described in the text. The energy of the ground state of the hydrogen atom is given by the intersection of this line with the oscillation frequency axis. (b) Time-time representation of the electron spectrogram obtained from Fourier analysis of the map shown in Fig. 2. The red vertical line indicates the temporal delay value corresponding to the crossing of the X-shaped region.

is given by

$$
I(\omega,t_d) = |M(\omega)|^2 = |M_1(\omega)|^2 + |M_2(\omega)|^2 \\
+ 2|M_1(\omega)M_2(\omega)| \cos \Delta\Phi(\omega,t_d), \quad (5)
$$

where $\Delta\Phi(\omega,t_d) = \phi_2(\omega) - \phi_1(\omega)$ is the phase difference between the two ionization paths. The spectral phase of the XUV pulses, obtained by calculating the Fourier transform of $\mathbf{A}_j(t)$, is given by

$$
\alpha_j(\omega_{\mathrm{XUV}}) = \omega_{\mathrm{XUV}}t_j + \frac{\xi_j\tau_j^2(\omega_{\mathrm{XUV}} - \omega_j)^2}{8\ln 2} \\
- \frac{1}{2}\arctan\xi_j - \varphi_j - \frac{\pi}{2}, \quad (6)
$$

where ω_{XUV} gives the XUV photon energy. We assume that the photon energy of the XUV pulses is above the ionization potential of the target atom, so that no resonant state is populated except for the ground state and the continuum states. Therefore, the spectral phase of the XUV pulses is directly mapped onto the free EWP [9], i.e., $\phi_j(\omega) = \alpha_j(\omega + I_p)$, thus leading to a phase difference $\Delta\Phi(\omega,t_d)$ given by the following expression:

$$
\Delta\Phi(\omega,t_d) = (\omega + I_p)t_d + \delta\zeta(\omega), \quad (7)
$$

where I_p is the ionization energy of the hydrogen atom and $\delta\zeta(\omega)$ is the chirp-dependent component of the phase difference. In the case of two XUV pulses with the same central carrier frequency, $\omega_0 \equiv \omega_1 = \omega_2$, and the same transform-
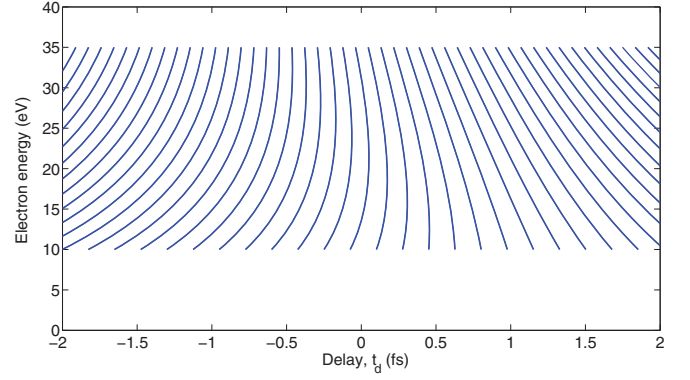
FIG. 4. (Color online) Analytical calculation of the interference fringe position of the electron spectrogram. The XUV pulse parameters are the same as in Fig. 2.

limited duration, $\tau \equiv \tau_1 = \tau_2$, $\delta\zeta(\omega)$ can be written as

$$
\delta\zeta(\omega) = \frac{(\xi_2 - \xi_1)\tau^2}{8\ln 2}(\omega - \omega_0 + I_p)^2 \\
+ \frac{1}{2}(\arctan\xi_1 - \arctan\xi_2) + (\varphi_1 - \varphi_2), \quad (8)
$$

which is a parabolic function of electron energy ω. Equation (5) shows that the spectrogram $I(\omega,t_d)$ is characterized by an interference structure with respect to ω and t_d. The position of the interference maxima is obtained from Eq. (7) and is given by $(\omega + I_p)t_d + \delta\zeta(\omega) = 2n\pi$ ($n = 0, \pm 1, \pm 2, \ldots$). We have directly solved the analytical equation to obtain the relationship between t_d and ω: the result is shown in Fig. 4. We note that the fringe position predicted by the analytical model is in excellent agreement with the TDSE calculation reported in Fig. 2.

In the energy-energy representation, the Fourier frequency ω' represents the oscillation frequency of $I(\omega,t_d)$ at a given electron energy ω. From Eqs. (5) and (7), we obtain that $\omega' = \omega + I_p$. This linear relation between ω and ω' is shown by the dashed line in Fig. 3(a), which can be seen as a linear fit of the TDSE numerical result. We note that the energy of the ground state of the hydrogen atom is directly given by the intersection of the line with the horizontal zero-energy line. This provides a method to measure the ground energy of the atom by the attosecond interference spectrogram. In the time-time representation, the electron energy ω is Fourier transformed to its conjugated time variable t. In this case, it is difficult to analytically investigate the relation between t and t_d, since ω is contained in all the terms of Eq. (5), where both $M_1(\omega)$ and $M_2(\omega)$ are unknown. To understand the effect of the frequency-dependent phase term $\delta\zeta(\omega)$ on the spectrogram in the time-time representation, we have considered the case of equal chirp rates ($\xi_1 = \xi_2 = 3$) while leaving all other parameters identical. In this way, the quadratic dependence of $\delta\zeta(\omega)$ with respect to ω is canceled. The calculated spectrogram in the time-time representation is shown in Fig. 5 and presents a structure similar to that reported in Fig. 3(b). The main difference between the two spectrograms is given by the value of the temporal delay corresponding to the crossing point of the X-shaped structure, indicated by the vertical dashed lines in Figs. 3(b) and 5. When the two
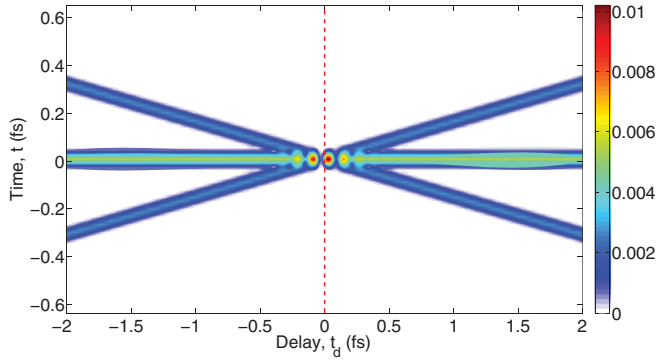
FIG. 5. (Color online) Time-time representation of the electron spectrogram, calculated for two attosecond pulses with the same chirp rate $\xi_1 = \xi_2 = 3$. All other pulse parameters are the same as in Fig. 2. The red vertical line indicates the temporal delay value corresponding to the crossing of the X-shaped region.

attosecond pulses have the same chirp rate, the crossing point of the X-shaped structure is located in correspondence with $t_d = 0$, whereas different chirp rates for the two pulses produce a shift of the crossing point: in the case reported in Fig. 3(b), the corresponding delay is $t_d = 120$ as. As a consequence, the use of two pulses with the same chirp allows one to calibrate the attosecond interferometer, since the crossing point identifies the zero-delay position. Hereafter, we can therefore assume that this position is known.

C. Reconstruction of quantum phase

The chirp-dependent phase term $\delta\zeta(\omega)$ can be completely retrieved from the interference pattern shown in Fig. 2. Figure 6(a) displays the DDIP as a function of the temporal delay for a particular electron energy value, $\mathcal{E}_0 = 20$ eV. The peak positions correspond to the condition of constructive interference: $\Delta\Phi(\omega,t_d) = 2n\pi$. We have then randomly selected five consecutive peaks [dashed rectangular box in Fig. 6(a)]: the corresponding phase $\Delta\Phi(\omega,t_d)$, which is denoted by the squares in Fig. 6(b), increases linearly with t_d. Note that a different choice of the consecutive peaks only leads to a phase shift by an integer multiple of 2π. Considering the numerical error, a linear fitting of the five squares is performed to obtain the temporal evolution of $\Delta\Phi(\omega,t_d)$, which is shown by the red-dashed line in Fig. 6(b). By extending this line to the zero-delay position, which is known in advance, it is possible to directly obtain $\delta\zeta(\omega)$ at the selected electron energy $\mathcal{E}_0$. Indeed, from Eq. (7), $\delta\zeta(\omega) = \Delta\Phi(\omega,0)$. Repeating the same procedure and selecting the same branches of the interference fringes for a series of electron energies, the phase term $\delta\zeta(\omega)$ can be obtained as a function of the electron energy. The retrieved phase values are shown in Fig. 7, together with the evolution of $\delta\zeta(\omega)$ calculated by using Eq. (8). The excellent agreement demonstrates that this approach successfully reconstructs the quantum phase $\delta\zeta(\omega)$. It is worth mentioning that the measurement of $\delta\zeta(\omega)$ only depends on the observable interference fringes, without requiring any prior information about the XUV pulses.

If the two XUV pulses have the same chirp rate, $\delta\zeta(\omega)$ does not depend on ω and it is given by $\delta\zeta(\omega) = \varphi_1 - \varphi_2$.
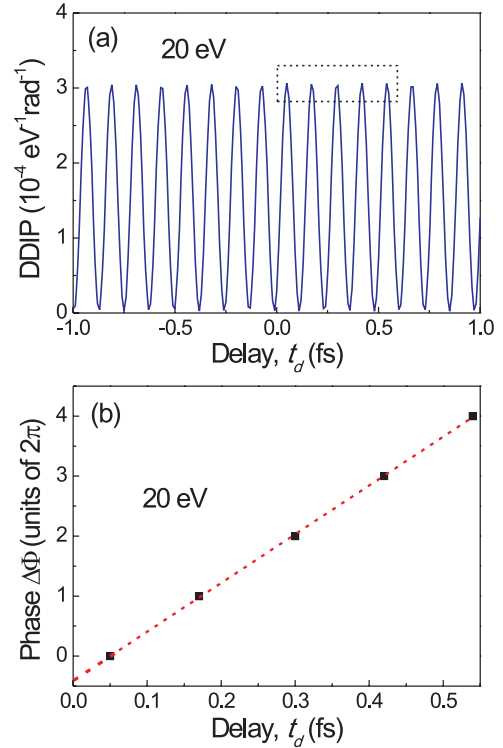
FIG. 6. (Color online) (a) DDIP as a function of the delay between the two attosecond pulses for a given electron energy $\mathcal{E}_0 = 20$ eV, directly extracted from Fig. 2. The dashed box shows the five peaks used for the reconstruction of the electron quantum phase as explained in the text. (b) Phase difference (squares), $\Delta\Phi(\omega,t_d)$, for the five peaks inside the dashed box of panel (a), as a function of the delay between the XUV pulses. The dashed line is the corresponding linear fitting curve.

Therefore, in this particular case, the measurement of the DDIP gives a direct method for the measurement of the relative CEP of two attosecond pulses. To further illustrate this point, we have calculated the interferogram in the case of two chirp-free attosecond pulses with three different pairs of CEP values: $\varphi_1 = \varphi_2 = 0$, $\varphi_1 = 0, \varphi_2 = \pi/2$, and $\varphi_1 = 0, \varphi_2 = 3\pi/2$. The retrieval procedure was then applied to obtain $\delta\zeta(\omega) \equiv \delta\zeta$.
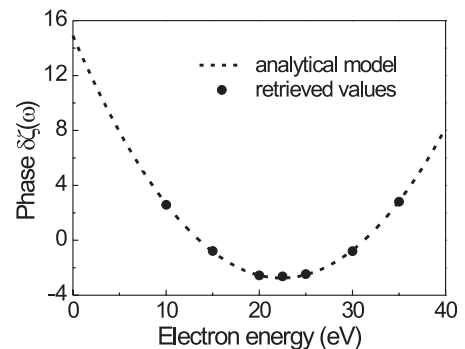
FIG. 7. Comparison of the phase term $\delta\zeta(\omega)$ calculated using the analytical model (dashed line), with the corresponding values (dots) obtained using the procedure illustrated in the text.
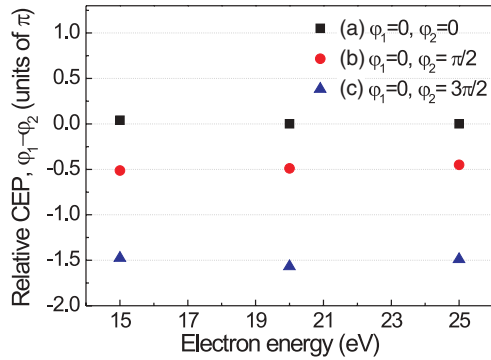
FIG. 8. (Color online) Difference between the CEP values of two chirp-free attosecond pulses used for the measurement of the electron spectrogram, retrieved using the procedure described in the text, in the case of three different electron energies ($\mathcal{E}_0 = 15$, 20, and 25 eV). Pulse parameters: $I_1 = I_2 = 1 \times 10^{12}$ W/cm^2, transform-limited duration $\tau_1 = \tau_2 = 130$ as (a) $\varphi_1 = \varphi_2 = 0$; (b) $\varphi_1 = 0, \varphi_2 = \pi/2$; and (c) $\varphi_1 = 0, \varphi_2 = 3\pi/2$.

The results are reported in Fig. 8 in the case of three different electron energies (15, 20, and 25 eV). The retrieved relative CEP values, defined by the average of the measured $\delta\zeta = \varphi_1 - \varphi_2$ values obtained for the different electron energies, are $\delta\zeta = 0.047$, $\delta\zeta = -0.483\pi$, and $\delta\zeta = -1.512\pi$, in excellent agreement with the expected values.

IV. CONCLUSIONS

We investigated the photoionization of a model hydrogen atom driven by two delayed attosecond pulses. The angular-resolved electron energy spectrum was calculated as a function of the temporal delay between the two pulses by numerically solving the fully 3D-TDSE. The calculated spectrogram shows a series of tilted fringes, whose energy spacing decreases as the delay increases. It was demonstrated that from the Fourier analysis of the electron spectrogram, it is possible to obtain the energy of the ground state of the target atom and a method for the identification of the zero time delay. Moreover, the intrinsic quantum phase difference of the two ionization channels involved in the continuum EWP can be completely retrieved from the measured spectrogram. This technique might provide promising avenues for complete reconstruction of the electron wave function of atoms. It was shown that the proposed interferometric technique allows one to measure the relative CEP value of two isolated attosecond pulses with the same chirp.

[1] P. M. Paul, E. S. Toma, P. Breger, G. Mullot, F. Augeé, Ph. Balcou, H. G. Muller, and P. Agostini, Science **292**, 1689 (2001).

[2] M. Hentschel, R. Kienberger, Ch. Spielmann, G. A. Reider, N. Milosevic, T. Brabec, P. B. Corkum, U. Heinzmann, M. Drescher, and F. Krausz, Nature (London) **414**, 509 (2001).

[3] F. Krausz and M. Ivanov, Rev. Mod. Phys. **81**, 163 (2009).

[4] M. Nisoli and G. Sansone, Prog. Quantum Electron. **33**, 17 (2009).

[5] P. Johnsson, J. Mauritsson, T. Remetter, A. L'Huillier, and K. J. Schafer, Phys. Rev. Lett. **99**, 233001 (2007).

[6] N. Shivaram, H. Timmers, X-M. Tong, and A. Sandhu, Phys. Rev. Lett. **108**, 193002 (2012).

[7] T. Remetter, P. Johnsson, J. Mauritsson, K. Varjú, Y. Ni, F. Lépine, E. Gustafsson, M. Kling, J. Khan, R. López-Martens, K. J. Schafer, M. J. J. Vrakking, and A. L'Huillier, Nat. Phys. **2**, 323 (2006).

[8] J. Mauritsson, T. Remetter, M. Swoboda, K. Klünder, A. L'Huillier, K. J. Schafer, O. Ghafur, F. Kelkensberg, W. Siu, P. Johnsson, M. J. J. Vrakking, I. Znakovskaya, T. Uphues,

S. Zherebtsov, M. F. Kling, F. Lépine, E. Benedetti, F. Ferrari, G. Sansone, and M. Nisoli, Phys. Rev. Lett. **105**, 053001 (2010).

[9] G. L. Yudin, A. D. Bandrauk, and P. B. Corkum, Phys. Rev. Lett. **96**, 063002 (2006).

[10] Y. Mairesse, A. de Bohan, L. J. Frasinski, H. Merdji, L. C. Dinu, P. Monchicourt, P. Breger, M. Kovačev, R. Taïeb, B. Carré, H. G. Muller, P. Agostini, and P. Saliéres, Science **302**, 1540 (2003).

[11] C. Liu, Z. Zeng, Y. Zheng, P. Liu, R. Li, and Z. Xu, Phys. Rev. A **85**, 043420 (2012).

[12] T. Nakajima and E. Cormier, Opt. Lett. **32**, 2879 (2007).

[13] C. Liu and M. Nisoli, Phys. Rev. A **85**, 053423 (2012).

[14] L. Roso-Franco, A. Sanpera, M. Ll. Pons, and L. Plaja, Phys. Rev. A **44**, 4652 (1991).

[15] E. S. Smyth, J. S. Parker, and K. T. Taylor, Comput. Phys. Commun. **114**, 1 (1998).

[16] G. Sansone, E. Benedetti, F. Calegari, C. Vozzi, L. Avaldi, R. Flammini, L. Poletto, P. Villoresi, C. Altucci, R. Velotta, S. Stagira, S. De Silvestri, and M. Nisoli, Science **314**, 443 (2006).